J. Fluid Mech. (2015), *vol.* 784, R6, doi:10.1017/jfm.2015.617

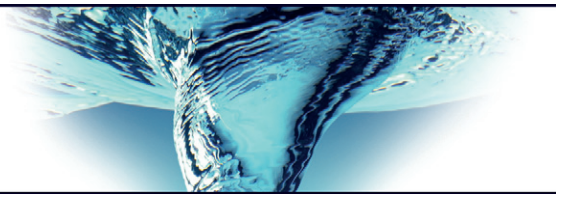

JFM RAPIDS
journals.cambridge.org/rapids

Experimental non-Boussinesq fountains

Rabah Mehaddi[1,†], **Olivier Vauquelin**[1] **and Fabien Candelier**[1]

[1]Aix-Marseille Université, Laboratoire IUSTI, UMR CNRS 7343, 5 rue Enrico Fermi, 13 453 Marseille, CEDEX 13, France

(Received 29 June 2015; revised 21 September 2015; accepted 19 October 2015; first published online 9 November 2015)

Laboratory experiments involving downward air–helium fountains are presented. The large density differences between these releases and the ambient allow us to investigate how non-Boussinesq effects modify fountain heights and fountain fluctuations in comparison with the Boussinesq case (i.e. marginal density differences). In these experiments, the source Froude number is varied over a wide range covering (i) the very weak, (ii) the weak and (iii) the forced fountain regimes. It is shown that the classical Boussinesq correlations can be extended to the non-Boussinesq case provided that the Froude number is multiplied by the square root of the ratio between the released fluid density and that of the ambient. In the range investigated, no influence of the source Reynolds number is observed.

Key words: convection, plumes/thermals

1. Introduction

A fountain, alternatively called a negatively buoyant jet, is a release whose buoyancy opposes its momentum. As illustrated in figure 1, at the initial stage of the fountain development, the release extends as a jet according to its initial momentum. Then, under the effects of the negative buoyancy, the local momentum decreases as the fountain rises until the local velocity vanishes at a given height. This height is called the transient height and is denoted here as H_{tr}. The flow then reverses direction and forms an annular down-flow which interacts with both the up-flow and the surrounding environment. Due to these interactions, the fountain height stabilises around a mean value (here referred to as H_m) generally lower than the transient height H_{tr}.

While the majority of studies have focused on Boussinesq fountains, for which densities are close to that of the ambient, fountains with significant density contrasts have received much less attention. To the best of our knowledge, the only available study in the literature concerning these non-Boussinesq fountains is that due to Baddour & Zhang (2009). In their experiments, carried out with hypersaline releases, these authors observed that the mean fountain heights were in general lower than

† Email address for correspondence: rabah.mehaddi@univ-lorraine.fr

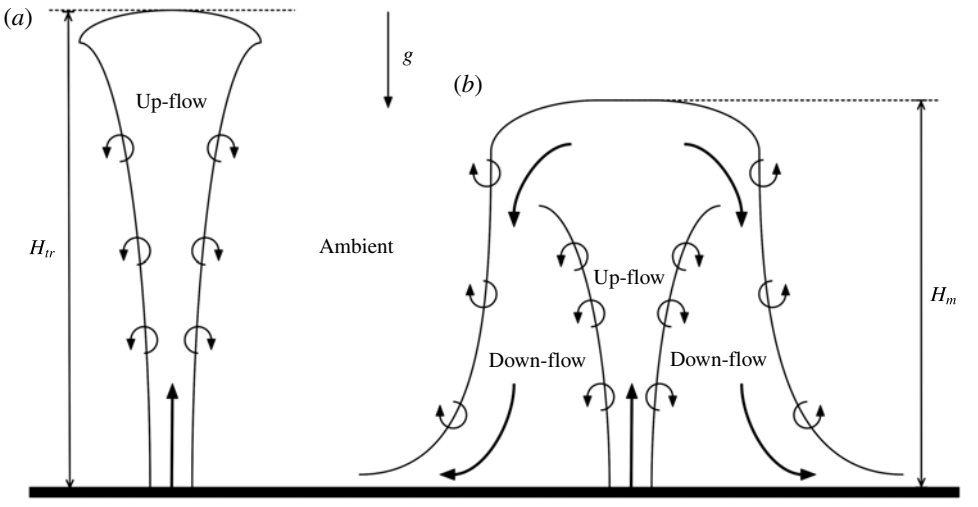

FIGURE 1. Schematic of the different steps of the development of a typical turbulent fountain: (*a*) initial up-flow, (*b*) steady state.

those predicted by using Boussinesq fountain correlations. They therefore concluded that these differences were related to non-Boussinesq effects.

In practice, experiments carried out with salt-water releases injected into fresh water do not allow a wide range of density contrast to be covered. This paper aims at extending the results by Baddour & Zhang (2009) by examining air–helium fountains. In particular, the objectives are to observe and to quantify how the mean fountain height H_m and its vertical oscillation frequency are affected by large density differences.

This paper is organised as follows. Section 2 presents some key results on Boussinesq fountains. The experimental set-up is described in § 3. In § 4, the results are analysed and new correlations for non-Boussinesq fountains are provided. Conclusions are drawn in § 5.

2. Key results on Boussinesq fountains

Let us first discuss some notable results on turbulent Boussinesq fountains.

One of the pioneering contributions is that due to Turner (1966). From both experimental and theoretical approaches, he found that the mean fountain height H_m and the transient fountain height H_{tr} (both divided by the radius of the source b_i) scale linearly with the source Froude number Fr:

$$\frac{H_m}{b_i} \simeq 2.46Fr \quad \text{and} \quad \frac{H_{tr}}{b_i} \simeq 3.52Fr. \tag{2.1a,b}$$

The Froude number, which quantifies the ratio between the buoyancy and the momentum at the source, is defined as follows:

$$Fr = \frac{w_i}{\sqrt{g\eta_i b_i}}, \tag{2.2}$$

where w_i is the bulk velocity of the released fluid, g is the gravitational acceleration and η_i is the source density deficit. Here, the density deficit is defined by

$$\eta_i = \frac{|\rho_i - \rho_0|}{\rho_0}, \tag{2.3}$$

where ρ_i is the density of the released fluid and ρ_0 is the ambient density. A striking result found by Turner (1966) is that the ratio H_m/H_{tr} remains constant and around 1.43.

As the range investigated by Turner (1966) was limited to high Froude numbers (i.e. forced fountains), Kaye & Hunt (2006) recently investigated low-Froude-number turbulent fountains. Their results exhibited the existence of two supplementary regimes: the weak fountain regime for which $H_m/b_i \propto Fr^2$ and the very weak fountain regime for which $H_m/b_i \propto Fr^{2/3}$. In the same vein, Burridge & Hunt (2012) studied the dynamics of salt-water Boussinesq fountains experimentally. Following an experimental approach similar to that used by Turner (1966), they found respectively for very weak, weak and forced fountains

$$\frac{H_m}{b_i} = 0.81Fr^{2/3} \quad \text{for } Fr < 1, \tag{2.4}$$

$$\frac{H_m}{b_i} = 0.86Fr^{2} \quad \text{for } 1 < Fr < 3, \tag{2.5}$$

$$\frac{H_m}{b_i} = 2.46Fr \quad \text{for } Fr > 3. \tag{2.6}$$

Burridge & Hunt (2013) also investigated the magnitude and the frequency of the fountain height oscillations around H_m. In the particular case of forced fountains, they exhibited the existence of a dominant frequency f which they used to build a Strouhal number ($St = fb_i/w_i$). This Strouhal number was found to scale as Fr^{-2}. The magnitude of the fountain fluctuations δz (divided by the source radius) was found to scale linearly with the Froude number.

We shall return to these Boussinesq results for comparison after describing the experimental set-up and the measurement methods.

3. Experimental apparatus

Figure 2 shows a sketch of the experimental apparatus. It is composed of a thin horizontal rectangular panel (1.5 m × 2.5 m). The panel is located 1.5 m from the floor of the laboratory, a distance that is sufficiently large to avoid any vertical confinement effect. To produce the fountains, a light air/helium mixture is continuously released downward from a nozzle of radius b_i, flush with the surface and located at the centre of the panel.

Before being released, the mixture first fills a large plenum chamber, located above the panel, which contains honeycomb sections. The air and helium flow rates are controlled by two independent flow meters. For low and moderate flow rates, Bronkhorst flow meters type EL-FLOW, which cover the range 0–12 $m^3\ h^{-1}$ with an accuracy of 2 % of the measurement, are used. For higher flow rates, Bronkhorst flow meters type E-7000, which cover the range 0–60 $m^3\ h^{-1}$ with an accuracy of 1 % of the measuring range, are used.

To visualise the flow, the released mixture is seeded with ammonium salt obtained by chemical reaction of ammonia vapour with hydrochloric acid. It should be noted that the mass of salt added to the flow is very weak and therefore does not affect the density of the fountain. A laser light sheet (argon 2 W) cuts through the central

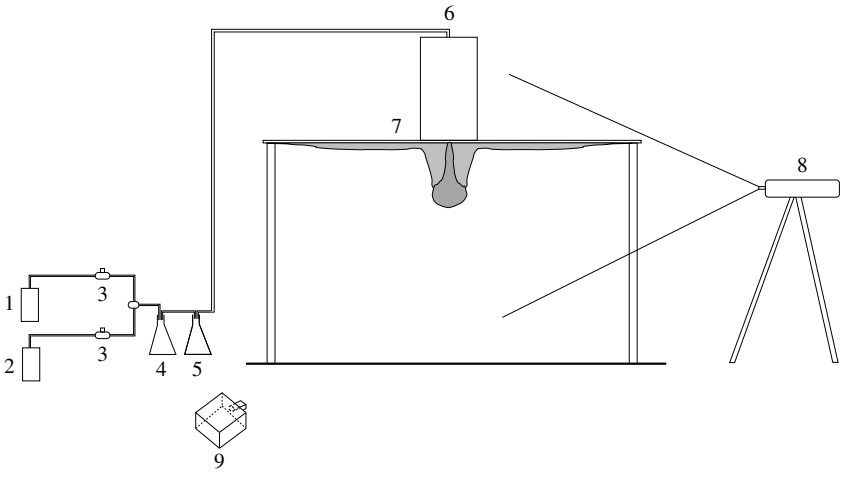

FIGURE 2. Schematic of the experimental apparatus: 1, air source; 2, helium source; 3, flow meters; 4, hydrochloric acid; 5, ammoniac; 6, plenum chamber; 7, rectangular panel; 8, laser sheet; 9, CCD camera.

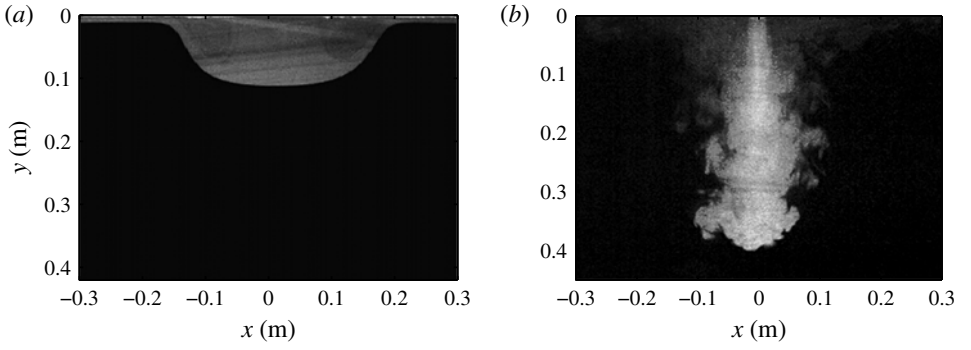

FIGURE 3. Instantaneous snapshots of (*a*) a stable fountain ($Fr = 1$, $Re = 570$ and $\rho_i/\rho_0 = 0.95$) and (*b*) a fluctuating fountain ($Fr = 14$, $Re = 1770$ and $\rho_i/\rho_0 = 0.44$).

plane of the fountain perpendicularly to the horizontal panel (see figure 3). Images are recorded as 8 bit bitmap image files at a frequency of 40 f.p.s. with a high-speed camera type PCO 1200hs equipped with a 50 mm Nikon lens.

For the experiments exploited in this paper, nine different nozzle diameters are used: 10, 20, 30, 38, 45, 84, 112, 118 and 138 mm. These diameters, together with the large density deficit range covered by air–helium mixtures, allow us to produce fountains with Froude numbers lying between 0.2 and 64 and Reynolds numbers lying between 120 and 3500. It should be noted that the (source) Reynolds number is defined by

$$Re = \frac{\rho_i w_i b_i}{\mu_i}, \tag{3.1}$$

where μ_i is the dynamic viscosity of the mixture. It should be noted that in our experiments, the ratio between the dynamic viscosity of the released fluid and that of the ambient air (i.e. μ_i/μ_{air}) lies between 1 and 1.12. According to this relatively

constant ratio, it can be assumed that the entrainment process will not be affected by the variation of the viscosity (see Campbell & Turner 1985).

To measure the mean fountain height H_m, recordings begin a while after the release reaches its steady-state phase. At least 2600 successive frames are recorded for each experiment in order to ensure statistical convergence of the measurements. The digital images are post-processed following an approach similar to those used by Williamson *et al.* (2008) and Burridge & Hunt (2012), which can be summarised as follows.

(1) Frames are read by using the software MATLAB® and converted in terms of grey level matrices. It should be noted that the values of the grey levels lie between 0 (black) and 255 (white).
(2) The matrices are then line-by-line averaged (i.e. horizontally averaged), producing vertical vectors of grey levels.
(3) These vertical vectors are concatenated to produce an image corresponding to a time series of rise heights for each fountain.
(4) The time evolution of the fountain height $H(t)$, from which both the mean height H_m and the fluctuations are measured, is extracted by using a light intensity threshold delimiting the fountain (white) envelope and the (black) surrounding.

It should be noted that, in this method, distances are measured with an accuracy of 4 pixels, corresponding to an actual distance of 5 mm in physical space.

Results are presented and compared with the Boussinesq correlations in the next section.

4. Observations and results

In this study 88 fountains have been investigated over the ranges $0.2 < Fr < 64$, $120 < Re < 3500$ and $0.13 < \rho_i/\rho_0 < 0.96$. These ranges allow us to cover transitional turbulent fountains (weak and forced) and laminar transitional fountains (weak and very weak). As expected, two different behaviours have been observed according to the values of the Froude number and the Reynolds number.

(1) For $Fr \lesssim 1$ and for a sufficiently small Reynolds number (typically $Re \lesssim 1000$), the fountain exhibits a stable aspect (see figure 3*a*). In this regime, a steady toroidal recirculating cell surrounding the base of the up-flow of the fountain is observed.
(2) For $Fr > 1$ and for a sufficiently high Reynolds number (typically $Re \gtrsim 1000$), the fountain exhibits a turbulent aspect (see figure 3*b*). In these cases, vertical oscillations of the fountain height around H_m are observed.

4.1. *Fountain mean heights*

We now focus on the influence of the density contrast (between the fountain and the ambient) on the mean fountain height. Figure 4 shows the experimental results together with the Boussinesq correlations (2.4), (2.5) and (2.6) corresponding to very weak, weak and forced fountain regimes respectively. In addition, in this figure, the data points are also shaded according to the value of the density ratio ρ_i/ρ_0 (light dots for weak density contrast and dark dots for strong density contrast). It is seen that some points deviate markedly from the Boussinesq correlations, especially when the density ratio ρ_i/ρ_0 is small (i.e. large density contrast). This is particularly true for forced fountains. This suggests non-Boussinesq effects.

To quantify these effects more precisely, let us first consider the experimental data corresponding to forced fountains ($Fr > 3$). To do so, the ratio $H_m/(2.46 b_i Fr)$ (bearing in mind that $2.46 b_i Fr$ corresponds to the mean height in the Boussinesq case) is plotted on a linear scale and on a log–log scale in figure 5 with respect to ρ_i/ρ_0.

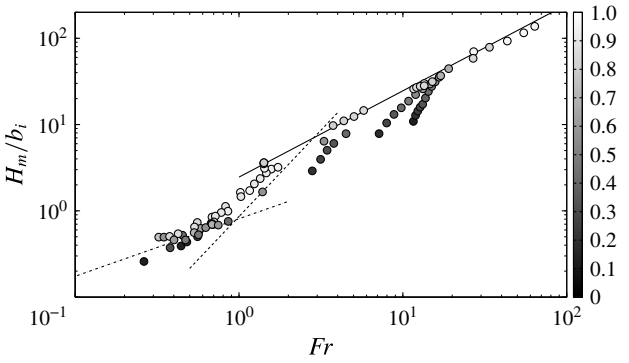

FIGURE 4. Comparisons between the present experimental results for the mean height H_m and the correlations by Burridge & Hunt (2012): solid line, $H_m/b_i = 2.46Fr$; dashed line, $H_m/b_i = 0.86Fr^2$; dash-dotted line, $H_m/b_i = 0.81Fr^{2/3}$. The experimental data points (○) are shaded according to the density ratio ρ_i/ρ_0.

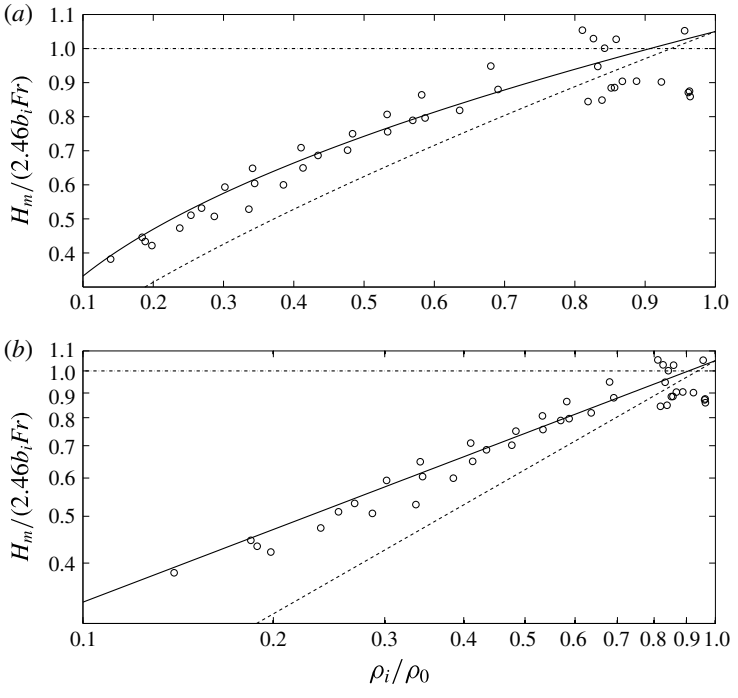

FIGURE 5. Determination from experimental data (○) the corrective function associated with the density ratio ρ_i/ρ_0. The solid line represents the best fit, with a slope of 1/2, and the dashed line, whose slope is 3/4, represents the solution derived from the Morton-like model (see appendix A). The dash-dotted line corresponds to the Boussinesq case.

As the ratio $H_m/(2.46b_iFr)$ is expected to be equal to 1 for Boussinesq fountains, any deviation from unity therefore provides insight into the role of non-Boussinesq effects. As expected, for weak density contrasts (i.e. $\rho_i/\rho_0 \to 1$), the experimental results are close to unity. However, for greater density contrasts (thus increasing the non-Boussinesq effects), the fountain reaches a mean height significantly weaker than

that predicted by the Boussinesq correlation. In particular, the deviation of the ratio $H_m/(2.46b_iFr)$ from unity clearly depends on the value of ρ_i/ρ_0. It turns out that the data points (see figure 5*b*) are scattered about a straight best-fit line (solid line) whose slope is close to 1/2. This best-fit relation reads as

$$\frac{H_m}{2.46b_iFr} \simeq 1.05\left(\frac{\rho_i}{\rho_0}\right)^{1/2} \quad \text{for } \frac{\rho_i}{\rho_0} < 0.8. \tag{4.1}$$

This is one of the main results of the present experimental study.

It should be noted that the present experimental results are in qualitative agreement with the recent experiments by Ahmad & Baddour (2015) carried out for upward turbulent fountains. Indeed, for a fixed value of the Froude number, these authors have shown that an increase of the density difference leads to a decrease of the fountain height.

Such a behaviour of the fountain height with respect to the density ratio seems to be not so obvious. In particular, it cannot be recovered by using a Morton-like theoretical approach in which the entrainment coefficient is modified to account for non-Boussinesq effects (as proposed by Ricou & Spalding (1961) or Rooney & Linden (1996) for turbulent plumes). To show this more clearly, the conservation equations applied to a rising fountain are solved in appendix A, leading us to a fountain height corrected with a density ratio to the power of 3/4. The Morton-like solution, given by (A 12), is then plotted in figure 5. It is seen that this approach overestimates the density effects. However, it is important to mention that the theoretical model presented in appendix A does not take into account the influence of the fountain down-flow. This is a possible explanation for the differences observed.

For convenience, the dependence on ρ_i/ρ_0 can be included in the definition of the non-Boussinesq Froude number,

$$Fr_{NB} = Fr\left(\frac{\rho_i}{\rho_0}\right)^{1/2} = \frac{w_i}{\sqrt{gb_i\bar{\eta}_i}}, \quad \text{where } \bar{\eta}_i = \frac{\rho_0 - \rho_i}{\rho_i}, \tag{4.2}$$

where the density difference $\bar{\eta}_i$ is made dimensionless by using ρ_i instead of ρ_0 (Boussinesq case). Introduction of such a non-Boussinesq Froude number indeed allows the dependence on both the density ratio ρ_i/ρ_0 and the Boussinesq source Froude number Fr to be captured. In particular, (4.1) can be simply rewritten as follows:

$$\frac{H_m}{b_i} \simeq 2.58Fr_{NB}. \tag{4.3}$$

It should be noted that to study turbulent plumes with large density contrasts, this non-Boussinesq Froude number has already been used by several authors, such as, for instance, Crapper & Baines (1978).

Relation (4.3) thus extends (2.6) to fountains with large density differences. In addition, we have also verified that in this regime, the fountain height does not depend on the source Reynolds number Re. Indeed, figure 6 shows the ratio $H_m/(2.58b_iFr_{NB})$ as a function of Re. We observe that all of the experimental points are close to unity despite a weak scattering, not exceeding 10 % for the lowest Reynolds number values. These results corroborate the findings of Philippe *et al.* (2005), who have exhibited experimentally the independence of the mean fountain height H_m on the source Reynolds number for $Re > 200$.

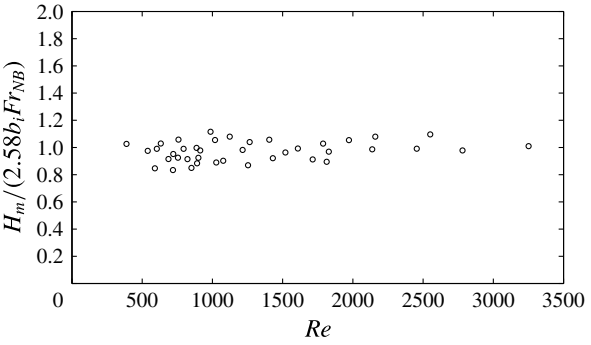

FIGURE 6. Ratio between the dimensionless fountain height and its corresponding correlation as a function of the source Reynolds number.

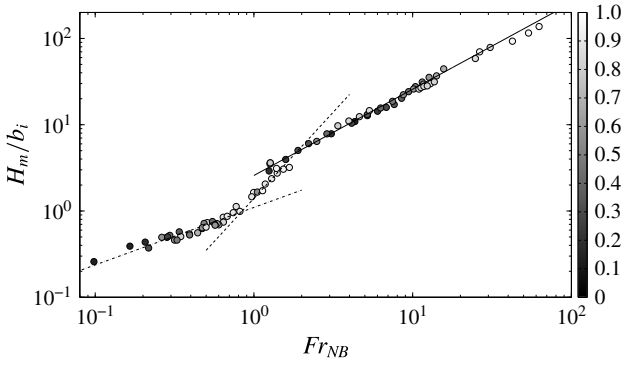

FIGURE 7. Comparisons between the experimental results obtained for the fountain mean height H_m and the following correlations: solid line, $H_m/b_i = 2.58Fr_{NB}$; dashed line, $H_m/b_i = 1.4Fr_{NB}^2$; dash-dotted line, $H_m/b_i = 1.1Fr_{NB}^{2/3}$. The data points (○) are shaded according to the density ratio ρ_i/ρ_0.

We now propose to plot in figure 7, for all of the experiments (i.e. including the very weak and weak regimes), the mean fountain height as a function of the non-Boussinesq Froude number Fr_{NB}. As expected, we observe that the experimental points in the forced regime align along the straight line corresponding to (4.3). It is remarkable, however, that for very weak and weak fountains, the experimental points also align with two straight lines (on a log–log scale) whose slopes are respectively 2/3 and 2. These two exponents are the same as those found by Burridge & Hunt (2012) for Boussinesq fountains. This leads us to the conclusion that the classical Boussinesq correlations concerning the mean fountain height can be straightforwardly generalised to the non-Boussinesq case by using Fr_{NB}. These new correlations are provided in table 1 with their specific ranges of validity given in terms of Fr_{NB}.

4.2. *Fountain fluctuations*

We now discuss the results concerning the fountain height fluctuations around H_m. Indeed, in some cases, the fountain height fluctuates due to self-sustained instabilities associated with the dynamics of the fountain collapsing on itself. For all experiments in which the fountain fluctuates, we determine first the standard deviation δz and

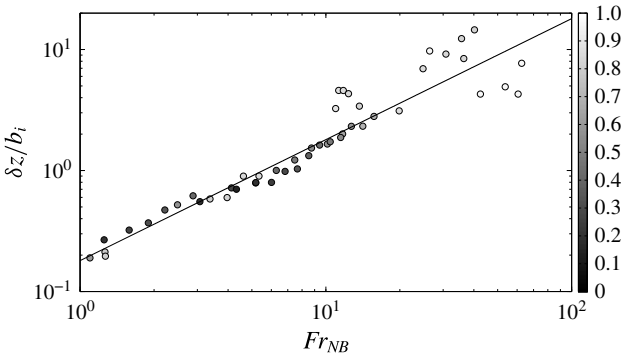

FIGURE 8. Variation of the standard deviation δz as a function of the non-Boussinesq Froude number Fr_{NB}. The best-fit line (solid line) is given by (4.4). The experimental data points (○) are shaded according to the density ratio ρ_i/ρ_0.

Regime	Fr_{NB}	Fountain mean height H_m/b_i
Very weak fountains	$0.1 < Fr_{NB} < 0.8$	$1.1Fr_{NB}^{2/3}$
Weak fountains	$0.8 < Fr_{NB} < 2$	$1.4Fr_{NB}^{2}$
Forced fountains	$Fr_{NB} > 2$	$2.58Fr_{NB}$

TABLE 1. Flow regime and the associated correlations for the mean fountain height as a function of the non-Boussinesq Froude number.

second the emerging frequency f from a Fourier transform analysis of the fountain height time signal $H(t)$.

Figure 8 shows the standard deviation δz versus Fr_{NB} in the case of forced fountains. The experimental data are best-fitted by the following linear relation:

$$\frac{\delta z}{b_i} \simeq 0.18 Fr_{NB}. \tag{4.4}$$

Again, this relation straightforwardly extends the Boussinesq correlation found by Burridge & Hunt (2012) (i.e. $\delta z/b_i \simeq 0.14Fr$) by using the non-Boussinesq Froude number.

To analyse the results concerning the emerging frequency f, let us reintroduce the Strouhal number St based on the source radius and the source velocity,

$$St = \frac{fb_i}{w_i}. \tag{4.5}$$

Figure 9 shows that, in the case of highly forced fountains ($Fr_{NB} \gg 1$), the Strouhal number is proportional to Fr_{NB}^{-2}. This dependence is similar to that found by Clanet (1998) (i.e. $St = 0.66Fr_{NB}^{-2}$) for non-miscible fountains (water in ambient air) as well as that found by Burridge & Hunt (2013) and Williamson *et al.* (2008) (i.e. $St \propto Fr^{-2}$) for Boussinesq fountains (salt-water into fresh water).

To analyse this dependence, let us recall that usually the initial source momentum M_i and the source buoyancy flux B_i are defined by

$$M_i = \frac{\rho_i}{\rho_0} w_i^2 b_i^2 \quad \text{and} \quad B_i = \frac{g(\rho_0 - \rho_i)}{\rho_0} w_i b_i^2. \tag{4.6a,b}$$

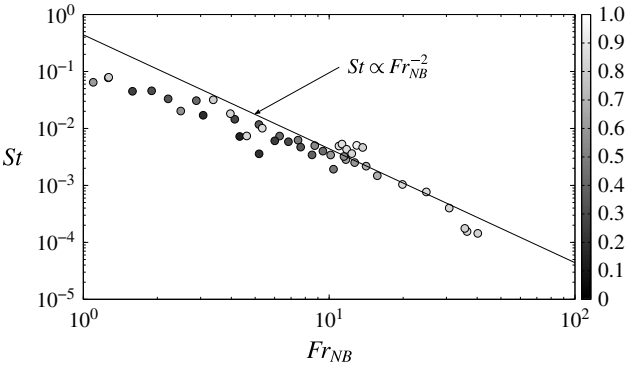

FIGURE 9. Variation of the Strouhal number St as a function of the non-Boussinesq Froude number Fr_{NB}. The experimental data points (○) are shaded according to the density ratio ρ_i/ρ_0.

According to the relation $St \propto Fr_{NB}^{-2}$, it can be inferred that

$$\frac{1}{f} \propto \frac{M_i}{B_i}. \tag{4.7}$$

As a result, this time scale is found to be independent of the radius of the fountain source. This is a common feature of elongated fountains (i.e. $H_m \gg b_i$), for which a radius-independent 'bobbing' behaviour is observed (see Vinoth & Panigrahi 2014).

5. Conclusions

In this paper, downward non-Boussinesq fountains have been investigated experimentally. To do so, air–helium mixtures have been released into the quiescent ambient air, allowing us to cover wide ranges of variation of the source Froude number, the source Reynolds number and the density ratio between the fountain and the surroundings (i.e. ρ_i/ρ_0).

The experimental results show that the (Boussinesq) classical relations concerning the steady mean fountain height and the rhythm of fountain fluctuations can be readily generalised to the non-Boussinesq case by using the non-Boussinesq source Froude number (see (4.2)).

This result is not so obvious. In particular, it cannot be derived by using a theoretical approach similar to that of Morton (1959) extended to the non-Boussinesq case, that is by multiplying the entrainment coefficient by the square root of the local density (see Ricou & Spalding 1961; Rooney & Linden 1996). Indeed, by introducing such a modified entrainment coefficient in the turbulent fountain equations (see appendix A), it turns out that the relation found reads as

$$\frac{H_m}{2.46 b_i Fr} \propto \left(\frac{\rho_i}{\rho_0}\right)^{3/4}, \tag{5.1}$$

which is different in nature from (4.1). It can therefore be concluded that such a theoretical approach overestimates the non-Boussinesq effects and, consequently, underestimates the fountain mean height, at least for downward fountains.

Appendix A

In this appendix, the height of a downward non-Boussinesq turbulent fountain is derived theoretically by using an approach inspired by Morton (1959). This approach is based on the conservation equations of volume, mass and momentum of the fountain flow (before the formation of the return flow), which are given respectively by

$$\frac{\mathrm{d}(wb^2)}{\mathrm{d}z} = 2\alpha\left(\frac{\rho}{\rho_0}\right)^{1/2} wb, \quad \frac{\mathrm{d}(\rho wb^2)}{\mathrm{d}z} = 2\alpha\left(\frac{\rho}{\rho_0}\right)^{1/2} \rho_0 wb, \quad \frac{\mathrm{d}(\rho w^2 b^2)}{\mathrm{d}z} = -g(\rho_0-\rho)b^2. \tag{A 1a–c}$$

Here, ρ_0 and ρ are respectively the densities of the ambient and of the fountain, b is the radius of the fountain, w is its vertical velocity, z is the vertical coordinate, the axis of which is oriented downward, and α is the entrainment coefficient. It should be noted that here the entrainment coefficient has been corrected with the square root of the local density, as is usually done for non-Boussinesq plumes (see Ricou & Spalding 1961; Rooney & Linden 1996).

To solve these equations, we introduce the functions Γ and β, which are defined as

$$\Gamma = \frac{5g(\rho_0-\rho)\beta}{8\rho\alpha w^2}, \quad \beta = b\left(\frac{\rho}{\rho_0}\right)^{1/2}. \tag{A 2a,b}$$

Derivation of these two functions with respect to the vertical coordinate leads us to

$$\frac{\mathrm{d}\Gamma}{\mathrm{d}z} = \frac{4\alpha\Gamma}{\beta}(\Gamma+1), \quad \frac{\mathrm{d}\beta}{\mathrm{d}z} = 2\alpha\left(1+\frac{2}{5}\Gamma\right). \tag{A 3a,b}$$

By combining these two equations, we obtain the following differential equation:

$$\frac{\mathrm{d}\Gamma}{\mathrm{d}z} = \frac{4\alpha}{\beta_i}\frac{\Gamma_i^{1/2}}{(1+\Gamma_i)^{3/10}}\Gamma^{1/2}(\Gamma+1)^{13/10}, \tag{A 4}$$

where β_i and Γ_i are the values of β and Γ at the source (i.e. $z=0$).

At the top of the fountain ($z=H_{tr}$), we have $w=0$ and $\Gamma\to\infty$. These two conditions allow the fountain height to be written in the following form:

$$\frac{H_{tr}}{\beta_i} = \frac{(1+\Gamma_i)^{3/10}}{4\alpha\Gamma_i^{1/2}}\int_{\Gamma_i}^{\infty}\Gamma^{-1/2}(\Gamma+1)^{-13/10}\,\mathrm{d}\Gamma. \tag{A 5}$$

To approximate (A 5) in the case of forced fountains (i.e. $\Gamma_i\to 0$), the prefactor can be expanded as

$$\frac{(1+\Gamma_i)^{3/10}}{4\alpha\Gamma_i^{1/2}} = \frac{1}{4}\frac{1}{\alpha\Gamma_i^{1/2}} + \frac{3}{40\alpha}\Gamma_i^{1/2} + O(\Gamma_i^{3/2}). \tag{A 6}$$

The integral in (A 5) is then split as follows:

$$\int_{\Gamma_i}^{\infty}\Gamma^{-1/2}(\Gamma+1)^{-13/10}\,\mathrm{d}\Gamma = \int_0^{\infty}\Gamma^{-1/2}(\Gamma+1)^{-13/10}\,\mathrm{d}\Gamma - \int_0^{\Gamma_i}\Gamma^{-1/2}(\Gamma+1)^{-13/10}\,\mathrm{d}\Gamma. \tag{A 7}$$

The first integral on the right-hand side of (A 7) evaluates to

$$\int_0^\infty \Gamma^{-1/2}(\Gamma+1)^{-13/10}\,\mathrm{d}\Gamma \approx 2.3. \tag{A 8}$$

Given that $\Gamma < \Gamma_i \ll 1$, the second integral on the right-hand side of (A 7) can be approximated as

$$\int_0^{\Gamma_i} \Gamma^{-1/2}(\Gamma+1)^{-13/10}\,\mathrm{d}\Gamma = \int_0^{\Gamma_i} \Gamma^{-1/2}\,\mathrm{d}\Gamma - \frac{13}{10}\int_0^{\Gamma_i} \Gamma^{1/2}\,\mathrm{d}\Gamma + O(\Gamma_i^{5/2}), \tag{A 9}$$

and we are led to

$$\int_0^{\Gamma_i} \Gamma^{-1/2}(\Gamma+1)^{-13/10}\,\mathrm{d}\Gamma = 2\Gamma_i^{1/2} - \frac{26}{30}\Gamma_i^{3/2} + O(\Gamma_i^{5/2}). \tag{A 10}$$

By combining (A 6), (A 8) and (A 10), we obtain

$$\lim_{\Gamma_i\to 0}\frac{H_{tr}}{\beta_i} = \frac{0.575}{\alpha\Gamma_i^{1/2}} - \frac{1}{2\alpha} + \frac{0.172}{\alpha}\Gamma_i^{1/2} + O(\Gamma_i). \tag{A 11}$$

At leading order, the dimensionless fountain height finally reads as

$$\frac{H_{tr}}{b_i} \approx \frac{0.575}{\alpha\Gamma_i^{1/2}}\left(\frac{\rho_i}{\rho_0}\right)^{1/2} \approx \frac{0.727}{\alpha^{1/2}} Fr\left(\frac{\rho_i}{\rho_0}\right)^{3/4}. \tag{A 12}$$

References

AHMAD, N. & BADDOUR, R. E. 2015 Density effects on dilution and height of vertical fountains. *J. Hydraul. Engng* **141** (11), 04015024.

BADDOUR, R. E. & ZHANG, H. 2009 Density effect on round turbulent hypersaline fountain. *J. Hydraul. Engng* **135**, 57–59.

BURRIDGE, H. C. & HUNT, G. R. 2012 The rise heights of low- and high-Froude-number turbulent axisymmetric fountains. *J. Fluid Mech.* **691**, 392–416.

BURRIDGE, H. C. & HUNT, G. R. 2013 The rhythm of fountains: the length and time scales of rise height fluctuations at low and high Froude numbers. *J. Fluid Mech.* **728**, 91–119.

CAMPBELL, I. H. & TURNER, J. S. 1985 Turbulent mixing between fluids with different viscosities. *Nature* **313** (5997), 39–42.

CLANET, C. 1998 On large-amplitude pulsating fountains. *J. Fluid Mech.* **366**, 333–350.

CRAPPER, P. F. & BAINES, W. D. 1978 Some remarks on non-Boussinesq forced plumes. *Atmos. Environ.* **12**, 1939–1941.

KAYE, N. B. & HUNT, G. R. 2006 Weak fountains. *J. Fluid Mech.* **558**, 319–328.

MORTON, B. R. 1959 Forced plumes. *J. Fluid Mech.* **5**, 151–163.

PHILIPPE, P., RAUFASTE, C., KUROWSKI, P. & PETITJEANS, P. 2005 Penetration of a negatively buoyant jet in a miscible liquid. *Phys. Fluids* **17**, 053601.

RICOU, F. P. & SPALDING, D. B. 1961 Measurements of entrainment by axisymmetrical turbulent jets. *J. Fluid Mech.* **11**, 21–32.

ROONEY, G. G. & LINDEN, P. F. 1996 Similarity considerations for non-Boussinesq plumes in an unstratified environment. *J. Fluid Mech.* **318**, 237–250.

TURNER, J. S. 1966 Jets and plumes with negative or reversing buoyancy. *J. Fluid Mech.* **26**, 779–792.

VINOTH, B. R. & PANIGRAHI, P. K. 2014 Characteristics of low Reynolds number non-Boussinesq fountains from non-circular sources. *Phys. Fluids* **26**, 014106.

WILLIAMSON, N., SRINARAYANA, N., ARMFIELD, S. W., MCBAIN, G. D. & LIN, W. 2008 Low-Reynolds-number fountain behaviour. *J. Fluid Mech.* **608**, 297–318.